

Multi-Atomic Mirror for Perfect Reflection of Single Photons in A Wide Band of Frequency

Yue Chang,¹ Z. R. Gong,^{1,*} and C. P. Sun^{1,†}

¹*Institute of Theoretical Physics, Chinese Academy of Sciences, Beijing, 100190, China*

A resonant two level atom doped in a one-dimensional waveguide behaves as a mirror, but this single-atom “mirror” can only reflect single photon perfectly at a specific frequency. For a one dimensional coupled-resonator waveguide, we propose to extend the perfect reflection region from a specific frequency point to a wide band by placing many atoms individually in the resonators in a finite coordinate region of the waveguide. Such a doped resonator array promises to control the propagation of a practical photon wave packet with certain momentum distribution instead of a single photon, which is ideally represented by a plane wave with specific momentum. The studies based on the discrete-coordinate scattering theory display that such hybrid structure with finite atoms indeed provides a near-perfect reflection for a single photon in a wide band. We also calculated the photon group velocity distribution, which shows that the perfect reflection wide band exactly corresponds to the stopping light region.

PACS numbers: 42.50.Ex, 03.65.Nk, 85.25.-j

I. INTRODUCTION

Quantum manipulation in all-optical fashions [1–4] is very crucial to the future development of high technology concerning optical communication [1, 5–10], quantum information process [1, 5, 7, 11, 12], and the next-generation quantum devices, e.g., single-photon transistors [5, 11, 13], quantum switches [1, 6–10, 13–15], and photon storages [2–4, 16, 17].

The core physics behind all-optical quantum manipulation is to explore the single-photon scattering and propagation in the confined structure of the sizes comparable to the wavelength of the photon. The investigations about the single-photon propagation in one-dimension involve some new phenomena, such as the perfect reflection of the single photon by atomic mirror [1, 6, 7, 14, 18], slowing light processes [2, 3, 16, 17, 19] in hybrid coupled-resonator waveguides, and other related issues [4–6, 9, 20]. The hybrid structures concerned here could be implemented physically with linear defect cavities in photonic crystals [21] with doped quantum dots, or superconducting transmission line resonators [8, 10, 15] coupled to a superconducting qubit [5, 22–25]. These physical systems with artificial band structures coupled to a two-level system enable us to control the transport of a single photon. By tuning the structure parameters of the hybrid system, the two-level system acts as a quantum switch, making the transporting single photon be reflected perfectly, or transmit totally. In this sense, the two-level system can behave as an ideal mirror [1, 6, 7, 14, 18].

It has been shown that a single-photon transistor using nanoscale surface plasmons [1] coupled with a three level atom in EIT (electromagnetically induced transparency) setup [2–4, 16, 17], exhibits controllable behavior in the transmission spectra. We have re-examined the coherent transport of a single photon in a coupled-resonator array coupled to a controllable two-level system [7]. Being different from the linear dispersion relation in Chang *et al.*'s setups [1, 6], the

cosine-type dispersion [7] will result in two bound-states in the hybrid system. The total reflection by the two-level system, which behaves as an ideal mirror, has been found associated with the Fano-Feshbach and Breit-Wigner line shapes [26] around the resonance in the reflection spectrum. However, in all these works [1, 6, 7], we emphasize that the perfect reflection exists only at a specific frequency point. It brings physical difficulties in practical applications, such as the efficiency to control an optical pulse, which actually is a superposition of the plane waves with different frequencies where the off-resonant components could deviate from the perfect reflection point dramatically.

In this paper, we propose an experimentally accessible setup based on the coupled-resonator array with doped atoms hybrid system, which is expected to realize perfect reflection with wide spectrum, and thus can perfectly reflect an optical pulse, namely, a single photon wave packet. Here, we use a “thick” atomic mirror which is made of an array of two-level atoms individually doped in some cavities arranged in a coordinate region of the one-dimensional coupled-cavity waveguide. The physical mechanism is intuitive: when a photon little far from resonance reaches one cavity coupled to the doped atom, it is reflected by the atom partly, and then the left part passing through the next atom experiences the same process. This process is repeated many times, which may realize the perfect reflection with wide spectrum so long as the interference enhancement could be suppressed by some mechanism. The emergence of wide-band spectrum is also shown schematically in Fig. 1, where the perfect reflection region is from a specific incident energy point (for single atom) to a wide band (for more than one atoms).

In details, we will study the wide-band scattering phenomena for our proposed atomic mirror by using the discrete coordinate scattering approach [7, 14]. Here, with the second order processes for the atom absorbing a photon and then radiating back inside cavity, the basic role of the doped atoms is to provide an effective potential like a local resonant Dirac comb [27], which leads to the stopping and slowing light phenomena [2, 3, 16, 17, 19]. By detuning the coupling strength of the atom coupled to the single cavity mode, we can feasibly control the width of the perfect reflection band. It is noticed

*Electronic address: gongzr@itp.ac.cn

†Electronic address: suncp@itp.ac.cn; URL: <http://www.itp.ac.cn/~suncp>

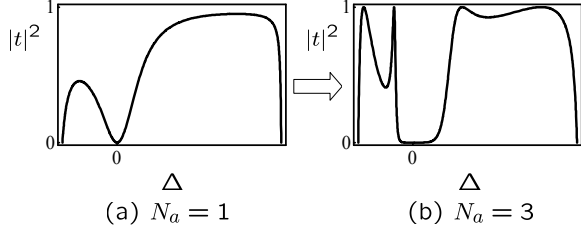


FIG. 1: Schematic diagram for the emergence of the wide band for perfect reflection. Here, Δ is the detuning concerning the incident photon's energy, and $|t|^2$ is the transmission coefficient. It is shown that for single atom [for (a)], the perfect reflection region is only a specific point; while when the atom number N_a is 3, the region is extended to a wide band.

that this wide-band spectrum phenomena have been implied in some works [14, 20, 28].

The paper is organized as follows. In Sec. II, we propose our model and solve it with the discrete coordinate scattering theory. In Sec. III, we study the microscopic physical mechanism and acquire the slowing light phenomenon in Sec. IV. In Sec. V, we study the influence of the imperfections in experiments on the perfect reflection wide-band. At last, we give a summary in Sec. VI.

II. WIDE-BAND ATOMIC MIRROR FOR SINGLE PHOTON IN ONE DIMENSION

Our hybrid system in this paper is shown in Fig. 2, where the N_a two-level atoms are individually embedded in a one-dimensional coupled-resonator waveguide (CRW) [29]. The atoms play essential role in controlling the propagation of a single photon. The Hamiltonian $H = H_c + H_I$ of this hybrid system consists of two parts, the CRW part described by a tight-binding boson model

$$H_c = \omega \sum_{j=-N}^N a_j^\dagger a_j + V \sum_{j=-N}^N (a_j^\dagger a_{j+1} + a_{j+1}^\dagger a_j), \quad (1)$$

and the part of two-level atoms interacting with the cavity fields

$$H_I = \frac{\Omega}{2} \sum_{j=1}^{N_a} (\sigma_j^z + 1) + g \sum_{j=1}^{N_a} (a_j \sigma_j^+ + a_j^\dagger \sigma_j^-). \quad (2)$$

Here, a_j is the annihilation operator of the j th single-mode cavity with frequency ω , and V is the hopping constant between the nearest neighbor cavities for the photon. We assume that all the two-level atoms and the cavity fields have the same energy level spacing Ω and frequency ω , respectively. The coupling between each atom and the corresponding cavity field is described by the Jaynes-Cummings model [30] with homogeneous coupling constant g . In Eq. (2), the Pauli spin matrices $\sigma_j^z \equiv |e\rangle_{jj}\langle e| - |g\rangle_{jj}\langle g|$ depicts the atomic energy of the j th atom with the ground state $|g\rangle_j$ and excited state $|e\rangle_j$, and $\sigma_j^+ \equiv (\sigma_j^-)^\dagger = |e\rangle_{jj}\langle g|$.

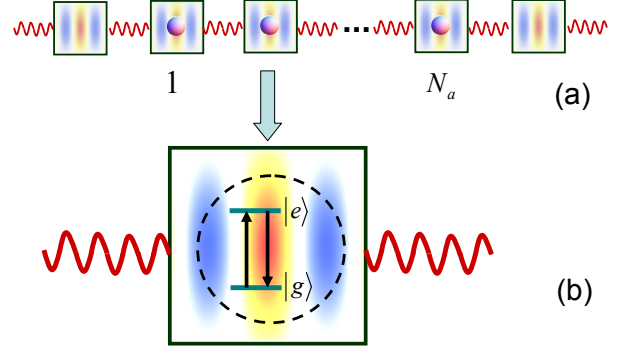


FIG. 2: (Color online) Schematic setup of the wide-band atomic mirror model. It is constituted by a coupled-resonator waveguide and an array of two-level atoms from 1 to N_a as shown in (a). The coupling between the cavity field and the two-level atom is shown in detail in (b), which is described by the Jaynes-Cummings model. The existence of the N_a atoms can extend the perfect reflection region to a wide band.

We note that the dispersion relation in the tight-binding boson model in Eq. (1) is the cosine-type, which results in bound states in the hybrid system. Actually, this tight-binding model is quite appropriate for simplifying the physical problem and has inspired extensive interests and lots of attentions both theoretically and experimentally [7, 8, 21, 31–34]. In our previous work [7], we have discovered that the electromagnetic field confined in this coupled-resonator waveguide can be well-controlled by a single two-level system.

To analyze the transport features of a single photon, we apply the discrete coordinate scattering approach [7, 14] by assuming the eigenstate of H with eigen-energy E for the incident photon in single excitation subspace as

$$|\Psi(E)\rangle = \sum_{j=-N}^N u_j^g |j\rangle \otimes |G\rangle + |0\rangle \otimes \sum_{j=1}^{N_a} u_j^e |e\rangle_j \otimes |G'_j\rangle, \quad (3)$$

where $|0\rangle$ represents the vacuum of the cavity fields, $|j\rangle = a_j^\dagger |0\rangle$, and

$$|G\rangle = \prod_{j=1}^{N_a} |g\rangle_j, |G'_j\rangle = \prod_{l=1, l \neq j}^{N_a} |g\rangle_l, \quad (4)$$

Here, u_j^g and u_j^e are the amplitudes of the single photon and the atomic population in the j th cavity, respectively. The first term on the right hand side of Eq. (3) depicts the single-photon propagating along the waveguide, while the second one represents that the photon is “captured” by an atom. It follows from the Schrödinger equation $H |\Psi(E)\rangle = E |\Psi(E)\rangle$ that the scattering equations for single photon with discrete coordinate representation read

$$\omega u_j^g + V (u_{j+1}^g + u_{j-1}^g) + W(E) u_j^g = E u_j^g. \quad (5)$$

Here, the effective potential

$$W(E) = w(E) \sum_{l=1}^{N_a} \delta_{jl} \quad (6)$$

is like a local resonant Dirac-comb [27] with strength $w(E) = g^2/(E - \Omega)$. The equations related to the atomic population are

$$\Omega u_j^e + g u_j^g = E u_j^e. \quad (7)$$

We indicate here that u_j^g and u_j^e in Eq. (3) depend on the energy E of the incident photon, and the interaction between the cavity fields and the atoms provides the potential $W(E)$ to affect the propagation of the single photon. Eq. (5) shows that due to the array of atoms, the incident single photon acquires an additional potential described by the local resonant Dirac comb, and the strength of this potential, i.e., $w(E)$, depends on the incident photon's energy E . On resonance, i.e., $E = \Omega$, the strength $w(E)$ of the effective potential is infinite, which definitely leads to the perfect reflection of the incident photon. This result is consistent with that in the previous work [7]. For the scattering in one dimension, in which the eigenfunction only possesses the reflection and transmission waves, the solutions to Eq. (5) for $j \neq 1, 2, \dots, N_a$ are supposed to be

$$u_j^g = \begin{cases} e^{ikj} + r e^{-ikj}, & j < 1 \\ t e^{ikj}, & j > N_a \end{cases}, \quad (8)$$

where r and t are reflection and transmission amplitudes respectively. To consider elastic scattering we can use the eigenvalue of the scattered photon

$$E(k) = \omega + 2V \cos k \quad (9)$$

with the cosine-type dispersion for the incident photon with momentum k .

The solutions in the region where the cavity fields interact with the atoms are supposed to be

$$u_j^g = r' e^{-ik'j} + t' e^{ik'j}, \quad (10)$$

for $j = 1, 2, \dots, N_a$, where k' is the solution of the transcendental equation

$$2V \cos k' = 2V \cos k - w(E), \quad (11)$$

which exhibits the conservation of energy. In Eqs. (8) and (10), r and t , together with r' and t' are determined below by four boundary conditions, i.e., the scattering equations (5) in four points $j = 0, 1, N_a, N_a + 1$. Then the transmission coefficient $|t|^2$ is obtained as

$$|t|^2 = \left| \frac{4V^2 \sin k \sin k'}{A(E)^2 e^{ik'(N_a-1)} - B(E)^2 e^{-ik'(N_a-1)}} \right|^2, \quad (12)$$

corresponding to the reflection coefficients $|r|^2 = 1 - |t|^2$, where

$$A(E) = V e^{-ik'} - V e^{-ik} + w(E), \quad (13)$$

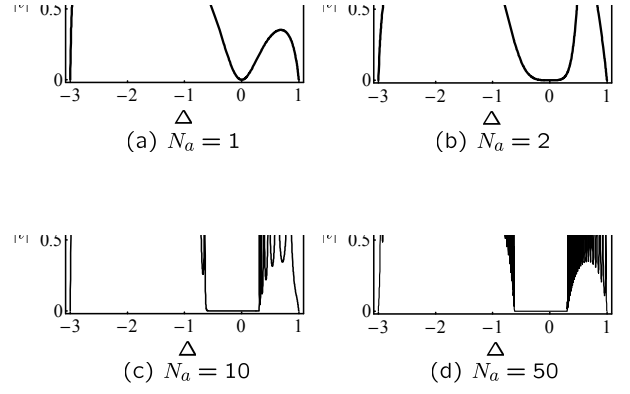


FIG. 3: The transmission spectrum $|t|^2$ as a function of the detuning Δ for different atom numbers N_a , where $N_a = 1$ [for (a)], $N_a = 2$ [for (b)], $N_a = 10$ [for (c)], and $N_a = 50$ [for (d)]. The wide-band of perfect reflection ($|t|^2 = 0$) emerges gradually as the atom number N_a increases. When doping only a few atoms (like $N_a = 10$), the near-perfect reflection band can fit the practical application. When the atom number N_a tends to infinite, the region of the wide-band reaches its maximum.

and

$$B(E) = V e^{ik'} - V e^{-ik} + w(E), \quad (14)$$

are independent of N_a .

Furthermore, it follows from Eq. (11) that, when

$$\left| \cos k - \frac{w(E)}{2V} \right| \geq 1, \quad (15)$$

k' is complex or $k' = n\pi$ (n is an integer), which exhibits the photon's probability decaying in the interaction region. When $k' = n\pi$, Eq. (12) gives that $|t|^2 = 0$. And when k' is complex, it is shown in Eq. (12) that $|t|^2 \rightarrow 0$ when $N_a \rightarrow +\infty$. In this case, the array of atoms behaves as a mirror that reflects the light perfectly.

The transmission spectra $|t|^2$ in Eq. (12) versus the detuning $\Delta = E(k) - \Omega$ for different atom numbers N_a are shown in Figs. 3(a)-3(d). The parameters in these figures are chosen as $\omega = 5g$, $\Omega = 6g$, and $V = -g$. These figures show that as N_a increases, the width of the perfect reflection band near the resonance $\Delta = 0$ increases correspondingly and at last reaches its maximum value with large N_a . In contrast to the single atom mirror case with only one specific reflection frequency, such multi-atom mirror can be used to manipulate the propagation of a practical wave packet, whose distribution in momentum space is restricted in the wide-band reflection region.

III. FREQUENT REFLECTIONS INDUCED SPECTRUM BROADENING

We have obtained the wide-band for perfect reflection by solving the discrete coordinate scattering equations (5) in the

last section. In this section, we study the physical mechanism of this wide-band and find the rigorous boundaries of the band.

As shown in Ref. [7], for single atom at the 0th single-mode cavity, the reflection and transmission amplitudes for single incident photon with momentum k are

$$r_1(k) = \frac{g^2}{-2iV(E - \Omega) \sin k - g^2} \quad (16)$$

and

$$t_1(k) = \frac{2iV(E - \Omega) \sin k}{2iV(E - \Omega) \sin k + g^2}, \quad (17)$$

respectively. The corresponding normalized eigenstate is

$$|\Omega(k)\rangle = \frac{1}{\sqrt{2\pi}} \sum_{j=-N}^N \xi_j^g a_j^\dagger |0\rangle |g\rangle_0 + \xi^e |0\rangle |e\rangle_0, \quad (18)$$

where

$$\xi_j^g(k) = \begin{cases} e^{ikj} + r_1(k) e^{-ikj}, & j < 0 \\ t_1(k) e^{ikj}, & j \geq 0 \end{cases} \quad \text{for } k > 0, \quad (19)$$

and

$$\xi_j^g(k) = \begin{cases} e^{ikj} + r_1(-k) e^{-ikj}, & j > 0 \\ t_1(-k) e^{ikj}, & j \leq 0 \end{cases} \quad \text{for } k < 0. \quad (20)$$

These reflection and transmission amplitudes are consistent in magnitudes with the results we have acquired in Eq. (12) when $N_a = 1$.

An element S_{kp} of the S -matrix describing the probability amplitude of an outgoing photon with momentum k when the incident photon momentum is p in this single-atom system is

$$S_{kp} = \delta_{kp} - i2\pi\delta_{E(k)E(p)} \langle k | V_{int} | \Omega(p) \rangle, \quad (21)$$

where

$$|k\rangle = \frac{1}{\sqrt{2\pi}} \sum_{j=-N}^N e^{ikj} a_j^\dagger |0\rangle |g\rangle_0 \quad (22)$$

is the outgoing state with momentum k ,

$$V_{int} = g \left(a_0 \sigma_0^+ + a_0^\dagger \sigma_0^- \right) \quad (23)$$

is the photon-atom coupling. Following these definitions, the S -matrix element reads

$$S_{kp} = \begin{cases} t_1(p) \delta_{kp} + r_1(p) \delta_{-k,p}, & p > 0 \\ t_1(-p) \delta_{kp} + r_1(-p) \delta_{-k,p}, & p < 0 \end{cases}. \quad (24)$$

Neglecting the interference between the reflection and transmission waves in the interaction region, the scattering matrix element $S'_{k,k}$ corresponding to the transmission amplitude for N_a atoms is written approximately as

$$S'_{k,k} \approx (S_{k,k})^{N_a} = t_1^{N_a}. \quad (25)$$

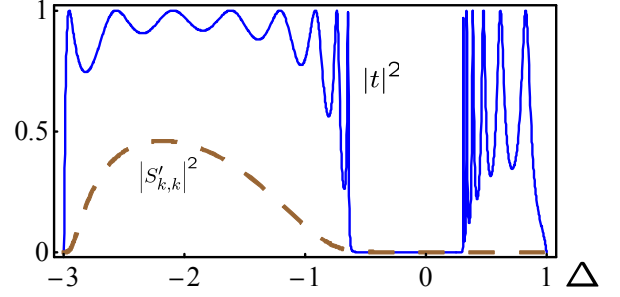


FIG. 4: (Color online) The transmission coefficient $|S'_{k,k}|^2 \equiv |t_1|^{2N_a}$ (brown dashed line) with respect to the detuning Δ in the approximation shown in Eq. (25) with $N_a = 10$. The other parameters are the same as that in Fig. 3. For comparison, the exact result $|t|^2$ (blue solid line) is plotted in this figure. It is shown that perfect reflection wide-bands appear in both $|S'_{k,k}|^2$ and $|t|^2$, which are due to the reflection of light by multi-atoms. The widths of these two band are different, as we do not take account of the interference of the reflection and transmission waves between different atoms in $|S'_{k,k}|^2$. Furthermore, the interference effect leads to the resonant transmission peaks in the transmission spectrum.

To investigate this approximation condition, we expand $|t|^2$ shown in Eq. (12) around the point $\Delta = 0$ as

$$|t|^2 \approx \left(\frac{V}{g^2} \right)^{2N_a} \frac{4V^2 - \delta^2}{V^2} \Delta^{2N_a} + o(\Delta^{2N_a}), \quad (26)$$

where we have made an approximation that $|2V \cos k| \ll |w(E)|$. With this expansion (26), we expand $|t_1|^{2N_a}$ approximately as

$$|t_1|^{2N_a} \approx \left(\frac{4V^2 - \delta^2}{g^4} \right)^{N_a} \Delta^{2N_a} + o(\Delta^{2N_a}). \quad (27)$$

It is shown in Eqs. (26) and (27) that in the region near the resonance, both $|t|^2$ and $|t_1|^{2N_a}$ tend to zero with the power-law function Δ^{2N_a} . Thus, it indicates that the emergence of the wide band near the resonance is due to the incoherent reflection by the array of atoms.

This approximate transmission coefficient is plotted in Fig. 4 in contrast with the rigorous solution shown in Fig. 3(c). Apparently, the wide-band perfect reflection phenomenon also appears in the approximate transmission coefficient. It demonstrates that the appearance of the wide-band is due to the reflection of light by the array of atoms. In other words, when the light reaches the first cavity coupled to a doped atom, the incident photon only has the probability $|t_1|^2$ to pass through the atom. And then, the second atom repeats this reflection process when the light passes through it and the transmission coefficient becomes $|t_1|^4$. This process is repeated by N_a atoms when the light passes through, and eventually leads to the transmission coefficient as $|t_1|^{2N_a}$. In this discussion, we do not take account of the interference effect at all, as the construction of the wide-band is only dominated by individual reflection processes. Actually, when considering the interference of reflection and transmission waves between atoms, the

region forbidding light propagation varies greatly. The interference effect also leads to the resonate transmission peaks in the transmission spectrum (see the peaks in Fig. 4).

The width of the perfect reflection band is determined by taking the imaginary part of the momentum k' nonzero or $k' = n\pi$. We notice that in Eq. (11), when

$$\cos k' = \frac{E - \omega - w(E)}{2V} \geq 1, \quad (28)$$

the wave vector k' is complex:

$$k'_+ = 2n_+\pi + i\alpha_+. \quad (29)$$

On the other hand, when

$$\cos k' = \frac{E - \omega - w(E)}{2V} \leq -1, \quad (30)$$

k' takes the form

$$k'_- = (2n_- + 1)\pi + i\alpha_-. \quad (31)$$

Here, n_{\pm} are integers and α_{\pm} are real. If k' has the form shown in Eq. (29) or (31), the denominator in Eq. (12) tends to infinity while N_a is sufficiently large, which results in the vanishing transmission coefficient.

It follows from Eqs. (28) and (30) that the range for the incident photon energy E is

$$\max\{E_-, E_{\min}\} \leq E \leq \min\{\Omega, E_{\max}\}, \quad (32)$$

or

$$\max\{\Omega, E_{\min}\} \leq E \leq \min\{E_+, E_{\max}\}, \quad (33)$$

where

$$E_{\pm} = \frac{1}{2}(\omega + \Omega) \mp |V| \pm \sqrt{\left(\frac{\delta}{2} \mp |V|\right)^2 + g^2}, \quad (34)$$

$$E_{\max} = \omega + 2|V|, E_{\min} = \omega - 2|V|, \quad (35)$$

and

$$\delta = \omega - \Omega. \quad (36)$$

When E is in this range determined by Eqs. (32) and (33), with lots of atoms, the photon is reflected perfectly.

When $g = 0$, the wide-band width $L = 0$, which corresponds to our common sense that the photon propagates free along the CRW without coupling to atoms. With the set of parameters in Fig. 3, the width L is $E_+ - E_-$, with the resonate point $\Delta = 0$ in the wide band. But note that with some other parameters, the point $\Delta = 0$ does not locate inside the wide-band. Additionally, when parameters satisfy one of the conditions as follows: (i) $E_- \leq E_{\min} \leq \Omega \leq E_{\max} \leq E_+$; (ii) $E_{\min} \geq \Omega$ and $E_+ \geq E_{\max}$; (iii) $E_{\min} \leq \Omega$ and $E_- < E_{\min}$, the band width is $4|V|$. Namely, by tuning the parameters in this region, the light can be reflected perfectly in the whole

V
(a)

g
(b)

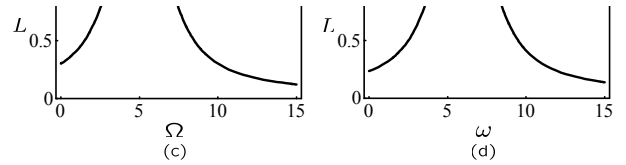


FIG. 5: The width L for the perfect reflection band as a function of the parameters V [for (a)], g [for (b)], Ω [for (c)], and ω [for (d)], with other parameters the same as that in Fig. 3. In Fig. 5(a), L firstly increases and then decreases with the increment of $|V|$. In Fig. 5(b), the width L increases as the atom-photon coupling strength $|g|$ increases, and L reaches its maximum $4|V|$ at last. In Figs. 5(c) and 5(d), in the region where the difference between the incident photon's energy and the atom's energy level spacing is very large, the width L tends to zero.

region of the energy of the incident photon. With other parameters the same as that in Fig. 3, we plot the wide-band width L with respect to the parameters V , g , Ω , ω respectively in Figs. 5(a)-5(d). It is shown in Fig. 5(a) that when $V = 0$, which means that the photon can not hop in the CRW, $L = 0$. As $|V|$ increases, L increases until $|V|$ reaches some critical point. Then L decreases when $|V|$ increases, since in this range, the larger the hopping strength $|V|$ is, the weaker the photon-atom coupling becomes as a perturbation. In Fig. 5(b), L is a monotonic increasing function of the atom-photon coupling strength $|g|$, and at last L reaches the maximum $4|V|$. Namely, the stronger coupling leads to a wider perfect reflection band. Eqs. 5(c) and 5(d) exhibit that when Ω or ω is very large, i.e., the difference between the incident photon's energy $E(k)$ and the two-level atom's energy level spacing Ω is very large, L tends to zero. The reason leading to this behavior is similar to that in the rotating-wave approximation [30], i.e., the large energy difference makes the interaction negligible with large time scale.

The width of the perfect reflection band is obtained with large N_a . We now discuss how large N_a is to insure our result

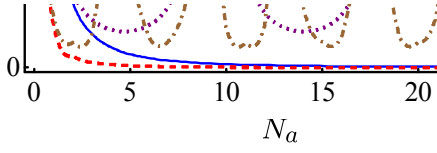


FIG. 6: (Color online) The transmission coefficients boundaries Δ_{\pm} with respect to N_a , where the blue dot represents $|t|^2$ in the left boundary, while the red dashed line represents $|t|^2$ in the right boundary. When $N_a \geq 20$, the transmission coefficients in both the two boundaries vanish approximately. As a result, the width we obtained of perfect reflection does not require $N_a \rightarrow \infty$ in practice. In fact, for the set of parameters in Fig. 6, $N_a = 20$ is large enough for the wide-band for perfect reflection. For comparison, the transmission coefficients with the energies beyond the wide band are plotted (the purple dotted line for $\Delta = -0.35$ and the brown dot-dashed line for $\Delta = 0.35$). The transmission $|t|^2$ does not tend to zero as the atom number N_a increases in the wide band.

reliable. With the parameters in Fig. 3, the boundaries of the wide-band are acquired using Eqs. (32) and (33).

$$\Delta_- \approx -0.618g \text{ and } \Delta_+ \approx 0.302g.$$

We plot the transmission coefficients $|t|^2$ in both boundaries with respect to N_a in Fig. 6. When N_a is large enough, the transmission coefficients in both boundaries vanish approximately. As a result, the width we obtained of perfect reflection does not require $N_a \rightarrow \infty$ in practice. In fact, for the set of parameters in Fig. 6, $N_a = 20$ is large enough for the wide-band for perfect reflection. For comparison, we plot $|t|^2$ versus N_a with the energies beyond the wide band, which show that $|t|^2$ does not tend to zero with the increment of N_a , even the energy is very close to that at the boundaries Δ_{\pm} .

IV. SLOW LIGHT RESONANT ABSORPTION

The wide-band reflection by multi-atom mirror has been shown above. Now we consider the slowing and stopping light phenomena in the interaction region with an array of atoms, which actually has a close relation to the emergence of the wide band [34].

We revisit the Hamiltonian in the interaction region

$$H_{int} = \sum_{j=1}^{N_a} \omega a_j^\dagger a_j + V \sum_{j=1}^{N_a-1} \left(a_j^\dagger a_{j+1} + a_{j+1}^\dagger a_j \right) + \sum_{j=1}^{N_a} \left[\frac{\Omega}{2} (\sigma_j^z + 1) + g (a_j \sigma_j^+ + a_j^\dagger \sigma_j^-) \right]. \quad (38)$$

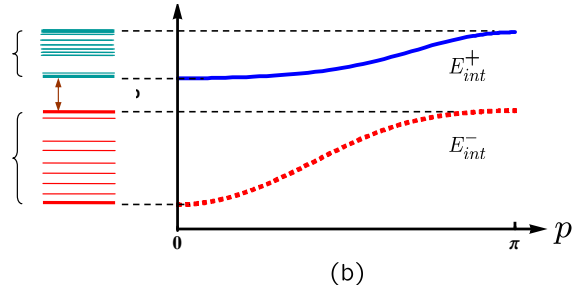


FIG. 7: (Color online) Schematic configuration for the two energy bands E_{int}^{\pm} [for (a)] and figure for $E_{int}^{\pm}(p)$ with respect to p [for (b)]. Each band has N_a energy levels, and when N_a energy levels tends to infinity, the band gap is $E^+ - E^-$.

The corresponding eigenstates for Eq. (38) is

$$|\Psi_{int}\rangle = \sum_{j=1}^{N_a} v_j^g |j\rangle \otimes |G\rangle + |0\rangle \sum_{j=1}^{N_a} v_j^e |e\rangle_j \otimes |G'_j\rangle, \quad (39)$$

with eigenvalue E that is determined by the set of equations

$$\omega v_j^g + V (v_{j+1}^g + v_{j-1}^g) + w(E) v_j^g = E v_j^g, \quad j = 2, \dots, N_a - 1, \quad (40)$$

$$\omega v_1^g + V v_1^g + w(E) v_1^g = E v_1^g, \quad (41)$$

$$\omega v_{N_a}^g + V v_{N_a-1}^g + w(E) v_{N_a}^g = E v_{N_a}^g, \quad (42)$$

and

$$\Omega v_j^e + g v_j^g = E v_j^e. \quad (43)$$

We note that the difference between Eqs. (40)-(42) and Eq. (5) is the different boundary conditions. The solutions to the set of equations (40)-(42) are

$$v_j^g = A \sin pj, \quad (44)$$

with normalization constant A , and the eigenvalues satisfy

$$E_{int} = \omega + \frac{g^2}{E_{int} - \Omega} + 2V \cos p, \quad (45)$$

where p is determined by the boundary conditions (41) and (42) as

$$p = \frac{n\pi}{N_a + 1}, \quad n = 1, \dots, N_a. \quad (46)$$

Consequently,

$$E_{int}^{\pm}(p) = \frac{1}{2} (\delta_p \pm \sqrt{\delta_p^2 + 4g^2}) + \Omega, \quad (47)$$

where $\delta_p = \delta + 2V \cos p$.

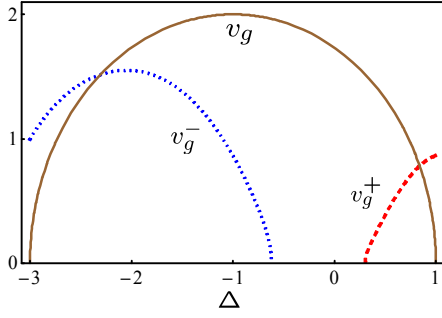


FIG. 8: (Color online) The light group velocity v_g^- (dotted blue line), v_g^+ (dashed red line), and v_g (solid brown line) for lower band E^- , upper band E^+ , and free tight-binding model $E(k)$ versus the detuning Δ . The region where $v_g^\pm = 0$ depicting the stopping light phenomenon exactly corresponds to the wide band for perfect reflection.

It is shown in Eq. (47) that there are two energy bands for the interaction region, which are labeled by E_{int}^+ and E_{int}^- . The two bands are shown schematically in Fig. 7(a). When N_a tends to infinity, the energy at bottom of the upper band E_{int}^+ is E_+ , and at top of the lower band E_{int}^- the energy is E_- , with the band gap $L = E_+ - E_-$ as shown in Eqs. (32) and (33). The band gap for the interaction region contains the wide band for perfect reflection of single photon. Namely, when the incident photon energy is in the band gap, it is impossible for the photon to go through the interaction region. With large N_a , we plot $E_{int}^\pm(p)$ with respect to p in Fig. 7(b). Here, the parameters are the same as that in Fig. 3. We note that the incident electron's energy corresponding to the resonant peaks in the transmission spectrum are not in agreement with the eigen-energies we obtained in Eq. (47) in the interaction region.

The group velocity v_g of light propagating in the interaction region is defined as

$$v_g^\pm(p) = \partial_p E_{int}^\pm(p). \quad (48)$$

Since the momentum k' in the interaction region depends on the energy E of the incident photon, the group velocity v_g is also dependent on E . However, when E is in the band gap, k' is complex, and $v_g(\Delta)$ is also complex. This complex $v_g(\Delta)$ depicts the decay in the light propagating in the interaction region. In this sense, when N_a is large, this group velocity is zero. It demonstrates that the stopping light phenomenon is due to the atomic mirror. The group velocities in the two bands are plotted in Fig. 8 with the same parameters in Fig. 3. For comparison, we also plot the group velocity $v_g = -2V \sin k$ in the CRW without doping atoms. When $\Delta < 0$, the photon propagates in the lower band, while $\Delta > 0$, the photon propagates in the upper band. Fig. 8 shows the slowing and stopping light phenomena in the interaction region, and the width of Δ in the light stopping region corresponds exactly to the width of the perfect reflection band shown in Fig. 3(d).

We note that these results based on the assumption that N_a is large, or even infinite. However, in practical applications,

N_a is finite and maybe not very large, so the reflection in the whole of the band would be not so perfect. We investigate the influence of N_a on the perfect reflection wide-band, and show that with some parameters, $N_a = 20$ is large enough to ensure the reliability of our results.

V. INFLUENCE OF IMPERFECTIONS IN EXPERIMENTAL IMPLEMENTS

In experiments, the atomic decay, the intrinsic loss of each coupled resonators, and the disorder [21, 35, 36] in the CRW, are inevitable. In this section, we investigate how these imperfections influence the frequency wide-band for perfect reflection we have studied. Firstly, we consider the disorder problem without atomic decay and losses of coupled resonators.

In principle, the whole CRW's scale can be infinite, thus we only consider a segment of disordered resonators. Moreover, we assume the disordered region happens to the atom-cavity interaction region, which means the hopping constant V_j for $i, j \in [1, N_a - 1]$, and the on-site frequency ω_j for $j \in [1, N_a]$ become position dependent. Under these assumptions, the total Hamiltonian

$$H_{imp} = H_L + H_{int}^D \quad (49)$$

is divided into two parts as: the leads' part

$$H_L = \omega \left(\sum_{j=-N}^0 + \sum_{j=N_a+1}^N \right) a_j^\dagger a_j + \quad (50)$$

$$V \left(\sum_{j=-N}^0 + \sum_{j=N_a}^N \right) (a_j^\dagger a_{j+1} + a_{j+1}^\dagger a_j), \quad (51)$$

and the disordered part in the atom-cavity interaction region

$$H_{int}^D = \sum_{j=1}^{N_a} \omega_j a_j^\dagger a_j + \sum_{j=1}^{N_a-1} V_j (a_j^\dagger a_{j+1} + a_{j+1}^\dagger a_j) + \sum_{j=1}^{N_a} \left[\frac{\Omega}{2} (\sigma_j^z + 1) + g (a_j \sigma_j^+ + a_j^\dagger \sigma_j^-) \right]. \quad (52)$$

The eigenstate of H_{imp} with eigen-energy $E = \omega + 2V \cos k$ for the incident photon with momentum k in single excitation subspace has the similar form of that in Eq. (3) as

$$|\Phi(E)\rangle = \left(\sum_{j=-N}^0 + \sum_{j=N_a+1}^N \right) \phi_j |j\rangle \otimes |G\rangle + |\Phi_D(E)\rangle, \quad (53)$$

where the amplitudes in leads part's wave-function can be still assumed to describe the reflection and transmission as

$$\phi_j = \begin{cases} e^{ikj} + r_D e^{-ikj}, & j < 1 \\ t_D e^{ikj}, & j > N_a \end{cases}, \quad (54)$$

and

$$|\Phi_D(E)\rangle = \sum_{j=1}^{N_a} \phi_j^g |j\rangle \otimes |G\rangle + |0\rangle \otimes \phi_j^e |e\rangle_j \otimes |G'_j\rangle \quad (55)$$

is the wave function in the atom-cavity interaction region. Here, r_L and t_L are the reflection and transmission amplitudes, respectively. Resulting from the continuous conditions of both the interfaces between the leads and the atom-cavity interaction region, those amplitudes satisfy

$$r_D = e^{ik} (\phi_1^g - e^{ik}), \quad (56)$$

$$t_D = e^{-ikN_a} \phi_{N_a}^g. \quad (57)$$

By solving the Schrodinger equation $H_{imp} |\Phi(E)\rangle = E |\Phi(E)\rangle$, we straightforwardly obtain the equation for $|\Phi_D(E)\rangle$ as

$$|\Phi_D(E)\rangle = V (e^{2ik} - 1) w |1\rangle \otimes |G\rangle, \quad (58)$$

where

$$w = \frac{1}{H_{int}^D + V e^{ik} (a_1^\dagger a_1 + a_{N_a}^\dagger a_{N_a}) - E}. \quad (59)$$

is the inverse of the Hamiltonian matrix together with the contributions of leads.

The amplitudes ϕ_1^g and $\phi_{N_a}^g$ are completely determined by the $2N_a \times 2N_a$ matrix w . Since the disorder exists in atom-cavity interaction region, the inhomogeneity of the hopping constants $\{V_j\}$ and on-site frequencies $\{\omega_j\}$ are expected to destroy the coherence of the incident photon and hence enhances the reflection. For a particular realization of disorder, i.e., for given sets $\{\omega_j\}$ and $\{V_j\}$ which are generated randomly in the ranges $[\omega - 0.2\omega, \omega + 0.2\omega]$ and $[V - 0.2V, V + 0.2V]$ respectively, we plot the transmission coefficient $|t_D|^2$ versus the detuning $\Delta = E(k) - \Omega$ in Fig. 9(a). Other parameters are the same as that in Fig. 3(c). Fig. 9(a) shows that the wide-band is almost not affected, while out the wide-band the transmission coefficient is changed dramatically. We assume the disorder in the atom-cavity interaction region has the Gaussian distribution of both $\{\omega_j\}$ and $\{V_j\}$ as

$$P(x) = \frac{\exp[-(x - x_0)^2/2\sigma^2]}{\sqrt{2\pi}\sigma}, \quad (60)$$

where $P(x)$ is the probability for a given value x , $x = \omega_j, V_j$, x_0 is the averaged value, and σ is the variance. We plot the averaged transmission coefficient $|t_D|^2$ versus Δ in Fig. 9(b)-(d). Here, for the sets $\{\omega_j\}$ and $\{V_j\}$, $x_0 = \omega$ and V , and the variances are respectively 0.01ω and $0.01|V|$ for Fig. 9(b), 0.05ω and $0.05|V|$ for Fig. 9(c), 0.1ω and $0.1|V|$ for Fig. 9(d). It is shown that Fig. 9(b) is quite similar to Fig. 3(c), both in the perfect and non-perfect reflection region. When the variances of $\{\omega_j\}$ and $\{V_j\}$ increase, the range of the wide-band is shortened, and in other region, the transmission curve is smoothed, with the depressed envelop, which demonstrates the destruction of the coherence of the incident photon due to the existence of the disorder.

The atomic decay and the loss of resonators also play essential role in experiments. Usually, such atomic decay and resonator losses mean inelastic scattering which results from

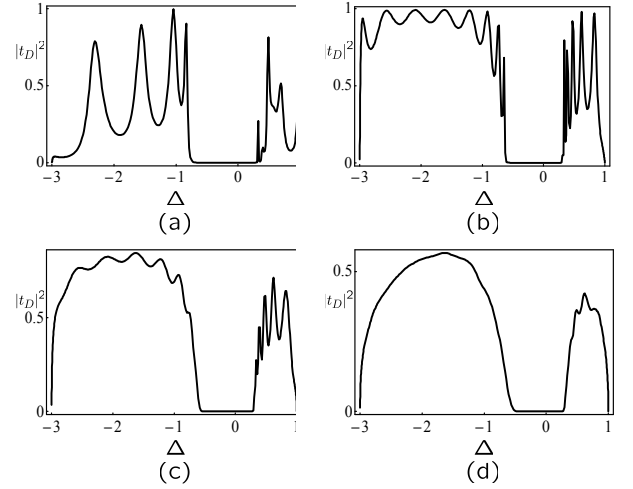


FIG. 9: The transmission coefficient $|t_D|^2$ as a function of the detuning Δ when the frequencies $\{\omega_j\}$ of the cavities and the coupling strength $\{V_{ij}\}$ between the nearest two cavities are different from site to site due to disorder. For given sets $\{\omega_j\}$ and $\{V_{ij}\}$ [for (a)], the wide-band for perfect reflection is almost unchanged while $|t_D|^2$ changes dramatically out of the wide-band. Figs. 9(b)-9(d) show the averaged results of the $\{\omega_j\}$ and $\{V_{ij}\}$ when the distributions of $\{\omega_j\}$ and $\{V_{ij}\}$ are Gaussian with the same mean values ω and V , but different variances. When the variances of $\{\omega_j\}$ and $\{V_{ij}\}$ are sufficiently small, e.g., 0.01ω and $0.01|V|$ [for (b)], the transmission curve is quite similar to that in Fig. 3(c). When the variances are increased, e.g., to 0.05ω and $0.05|V|$ [for (c)], and 0.1ω and $0.1|V|$ [for (d)], the range of the wide-band is shortened, and in other region, the transmission curve is smoothed, with the depressed envelop, which demonstrates the destruction of the coherence of the incident photon due to the existence of the disorder.

the interaction between the system and a realistic environment described by phonons. For simplicity, we investigate this effect on the perfect reflection wide-band by phenomenologically adding imaginary parts $-i\gamma_a$ and $-i\gamma_c$ to the two-level atom's frequency Ω and coupled resonators' frequency ω , respectively. We note that these losses will can be directly added in the final results (see Eq. (12)) phenomenologically. As a result, without disorders, the transmission coefficient in Eq. (12) becomes

$$|t_L|^2 = \left| \frac{4V^2 \sin k \sin k'_L}{C(E_L)^2 e^{ik'_L(N_a-1)} - D(E_L)^2 e^{-ik'_L(N_a-1)}} \right|^2, \quad (61)$$

where

$$C(E_L) = V e^{-ik'_L} - V e^{-ik} + w_L(E_L), \quad (62)$$

$$D(E_L) = V e^{ik'_L} - V e^{-ik} + w_L(E_L), \quad (63)$$

and k'_L satisfies the equation

$$2V \cos k'_L = 2V \cos k - w_L(E). \quad (64)$$

Here, $w_L(E_L) = g^2 / [E_L - (\Omega - i\gamma_a)]$ and $E_L = \omega - i\gamma_c +$

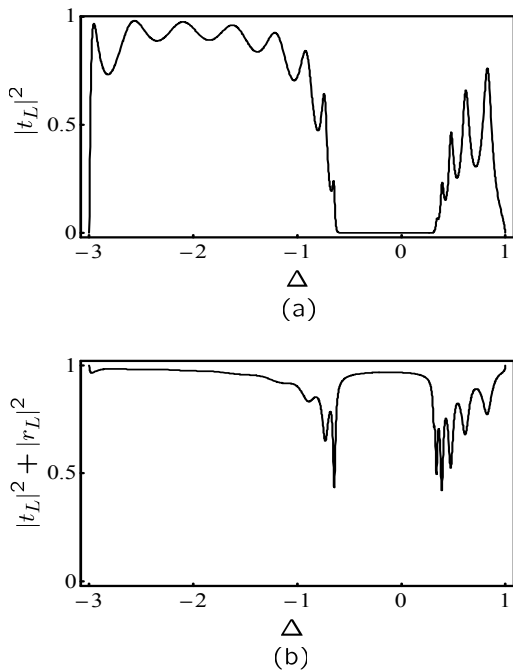


FIG. 10: The transmission coefficient $|t_L|^2$ [for (a)] and $|r_L|^2 + |t_L|^2$ [for (b)] with respect to the detuning Δ in the system-environment interacting case. It is shown that the perfect reflection band still exist, and the photon current is no more conserved.

$2V \cos k$. The corresponding reflection coefficient is

$$|r_L|^2 = \left| i2V \sin k \frac{C(E_L) - D(E_L)e^{-i2k'_L(N_a-1)}}{C(E_L)^2 - D(E_L)^2 e^{-i2k'_L(N_a-1)}} - 1 \right|^2, \quad (65)$$

With the same parameters in Fig. 3(c), we plot the transmission spectrum $|t_L|^2$ and $|r_L|^2 + |t_L|^2$ in Fig. 10, where $\gamma_a = 0.02g$ and $\gamma_c = 0.01g$. It is shown in Fig. 10(a) that the wide-band for perfect reflection also exists in the transmission spectrum, with almost the same boundaries when γ_a/Ω , $\gamma_c/\omega \ll 1$, and $\gamma_a > \gamma_c$ are satisfied, but the envelop of the transmission curve is depressed globally. This phenomenon also appears in Fig. 10(b), which exhibits that the photon

current is not conserved any more, especially near the two boundaries Δ_{\pm} . However, when the single photon stops in the interaction region, the energy is almost conserved. From the above discussion,, the wide-band for near-perfect reflection is almost not influenced by the imperfections such as disorder, atomic decay and resonator losses existing in the realistic experiments..

VI. SUMMARY

We have studied the coherent transport of a single photon in a one-dimension array of coupled-resonators individually coupled to two-level atoms. The discrete coordinate scattering approach shows that a wide-band spectrum appears for perfect reflection when the number of atoms N_a is large. The physical mechanism for this wide-band is considered by the incoherent multi-reflection for light by N_a atoms, which extends the perfect reflection line to form a wide band. The slowing and stopping light phenomena also appear due to the interaction with atoms. We also diagonalize exactly the photon-atoms interaction Hamiltonian in the interaction region, and obtain two energy bands. It is found that the perfect reflection wide-band is embedded in this band gap. We also consider the effect of imperfections in experimental implements and find that the wide-band for near-perfect reflection is not influenced when the parameters describing the imperfections are small.

The model we proposed here can be realized by a circuit QED system [5, 22–24], where the CRW can be realized by either defect resonators in photonic crystals [21] or coupled superconducting transmission line resonators [8, 10, 15]. By engineering the photon-atoms coupling strengths and other parameters such as the hopping constant and the energy space between the two levels of the atoms, we can control the width and position of the perfect reflection wide band.

Acknowledgments

The work is supported by NSFC No. 10474104, 60433050, and No. 10704023, NFRPC No. 2006CB921205 and 2005CB724508.

[1] D. E. Chang, A. S. Sørensen, E. A. Demler, and M. D. Lukin, *Nat. Phys.* **3**, 807 (2007).
 [2] C. P. Sun, Y. Li, and X. F. Liu, *Phys. Rev. Lett.* **91**, 147903 (2003).
 [3] Y. Li and C. P. Sun, *Phys. Rev. A* **69**, 051802(R) (2004).
 [4] Z. R. Gong, H. Ian, Lan Zhou, and C. P. Sun, *Phys. Rev. A* **78**, 053806 (2008).
 [5] A. Wallraff, D. I. Schuster, A. Blais, L. Frunzio, R.- S. Huang, J. Majer, S. Kumar, S. M. Girvin, and R. J. Schoelkopf, *Nature (London)* **431**, 162 (2004).
 [6] J. T. Shen and S. Fan, *Phys. Rev. Lett.* **95**, 213001 (2005).
 [7] L. Zhou, Z. R. Gong, Yu-xi Liu, C. P. Sun, and F. Nori, *Phys.*

Rev. Lett. **101**, 100501 (2008).
 [8] L. Zhou, Y. B. Gao, Z. Song, and C. P. Sun, *Phys. Rev. A* **77**, 013831 (2008).
 [9] L. Zhou, S. Yang, Yu-xi Liu, C. P. Sun, and F. Nori, *Phys. Rev. A* **80**, 062109 (2009).
 [10] J. Q. Liao, Z. R. Gong, L. Zhou, Yu-xi Liu, C. P. Sun, and F. Nori, *Phys. Rev. A* **81**, 042304 (2010).
 [11] M. Hijlkema, B. Weber, H. P. Specht, S. C. Webster, A. Kuhn, and G. Rempe, *Nat. Phys.* **3**, 253 (2007).
 [12] D. Bouwmeester, A. Ekert, and A. Zeilinger, *The Physics of Quantum Information* (Springer, Berlin, 2000).
 [13] M. Orrit, *Nat. Phys.* **3**, 755 (2007).

- [14] L. Zhou, H. Dong, Yu-xi Liu, C. P. Sun, and F. Nori, Phys. Rev. A **78**, 063827 (2008).
- [15] J. Q. Liao, J. F. Huang, Yu-xi Liu, L. M. Kuang, and C. P. Sun, Phys. Rev. A **80**, 014301 (2009).
- [16] D. L. Zhou, Lan Zhou, R. Q. Wang, S. Yi, and C. P. Sun, Phys. Rev. A **76**, 055801 (2007).
- [17] L. Zhou, J. Lu, D. L. Zhou, and C. P. Sun, Phys. Rev. A **77**, 023816 (2008).
- [18] M. Olshanii, Phys. Rev. Lett. **81**, 938 (1998).
- [19] M. Patterson *et al.*, Phys. Rev. Lett. **102**, 253903 (2009).
- [20] T. S. Tsoi and C. K. Law, Phys. Rev. A **78**, 063832 (2008).
- [21] A. D. Greentree, C. Tahan, J. H. Cole, and L. C. L. Hollenberg, Nat. Phys. **2**, 856 (2006).
- [22] J. Q. You and F. Nori, Phys. Rev. B **68**, 064509 (2003).
- [23] J. Q. You, J. S. Tsai, and F. Nori, Phys. Rev. B **68**, 024510 (2003).
- [24] I. Chiorescu, P. Bertet, K. Semba, Y. Nakamura, C. J. P. M. Harmans, and J. E. Mooij, Nature (London) **431**, 159 (2004).
- [25] J. Q. You and F. Nori, Phys. Today **58**, No. 11, 42 (2005).
- [26] L. D. Landau and E. M. Lifshitz, *Quantum Mechanics (Nonrelativistic Theory)* (Butterworth, Boston, 1991).
- [27] S. Flügge, *Practical Quantum Mechanics* (Springer-Verlag, Berlin, 1999).
- [28] M. Patterson, S. Hughes, arXiv:1002.4208v1.
- [29] K. Y. Bliokh, Y. P. Bliokh, V. Freilikher, S. Savel'ev, and F. Nori, Rev. Mod. Phys. **80**, 1201 (2008).
- [30] D. F. Walls and G. J. Milburn, *Quantum Optics* (Springer-Verlag, Berlin, 1994).
- [31] M. F. Yanik and S. Fan, Phys. Rev. Lett. **92**, 083901 (2004).
- [32] M. F. Yanik and S. Fan, Phys. Rev. A **71**, 013803 (2005).
- [33] L. Zhou, J. Lu, and C. P. Sun, Phys. Rev. A **76**, 012313 (2007).
- [34] F. M. Hu, L. Zhou, T. Shi, and C. P. Sun, Phys. Rev. A **76**, 013819 (2007).
- [35] S. Mookherjea, Jung S. Park, Shun-Hui Yang, Prabhakar R. Bandaru, Nature Photonics **2**, 90 (2008).
- [36] J. Grgić, E. Campaioli, S. Raza, P. Bassi, N. A. Mortensen, Opt. Quant. Electron **5**, 10009 (2010).